applied sciences

Article

An Improved SOC-Adaptive Droop Control for DC Microgrids with Enhanced Utilization and Economic Performance

Xudong Wang [1], Saishuang Wang [2], Chunsheng Yang [3], Qisheng Wu [4], Zhigang Wei [5], Linyi Li [6], Jianglong Guo [7,*] and Weiyu Liu [4,*]

[1] School of Management and Economics, North China University of Water Resources and Electric Power, Zhengzhou 450046, China; wxd930205@163.com
[2] College of Electrical Engineering, North China University of Water Resources and Electric Power, Zhengzhou 450045, China; wangsaishuang@ncwu.edu.cn
[3] School of Mechanical Engineering, North China University of Water Resources and Electric Power, Zhengzhou 450045, China; 13592434238@163.com
[4] School of Electronics and Control Engineering, Chang'an University, Xi'an 710064, China; qshwu@chd.edu.cn
[5] China Northwest Architectural Design and Research Institute Co., Ltd., Xi'an 710018, China; sandy_na2000@sina.com
[6] State Grid Xinjiang Electric Power Research Institute, Urumqi 830013, China
[7] Xi'an Key Laboratory of Advanced Transport Power Machinery, School of Energy and Electrical Engineering, Chang'an University, Xi'an 710064, China
* Correspondence: 2024138029@chd.edu.cn (J.G.); liuweiyu@chd.edu.cn (W.L.)

Abstract

This paper proposes an improved state-of-charge (SOC)-based adaptive droop control strategy for photovoltaic DC microgrids with distributed energy storage units (DESUs). To overcome the slow SOC equalization and limited adaptability of conventional droop control methods, a nonlinear arctangent-based droop coefficient adjustment mechanism is introduced to enhance regulation sensitivity under small SOC deviations. In addition, a capacity compensation factor and an acceleration term are incorporated to improve proportional power sharing and SOC convergence speed among heterogeneous storage units. To further evaluate the engineering significance of SOC balancing performance, a time-integrated SOC deviation index is introduced to analyze the cumulative imbalance effect on battery degradation and lifecycle operation. By reducing the SOC imbalance duration, the proposed strategy contributes to mitigating uneven battery aging and may potentially reduce long-term battery replacement costs. Simulation results under discharging, charging, and irradiance-variation scenarios demonstrate that the proposed strategy significantly improves SOC-balancing performance compared with conventional SOC-based droop control. Across the three operating modes, the average SOC balancing time has been reduced by 52.6%. The proposed method provides an effective and economically sustainable control framework for distributed energy storage coordination in DC microgrids.

Keywords: SOC balance; droop control; energy storage system; DC microgrid; voltage compensation

Academic Editors: Antonio Maffucci and Paolo Renna

Received: 31 May 2026
Revised: 13 July 2026
Accepted: 17 July 2026
Published: 22 July 2026

1. Introduction

DC microgrids have gained increasing attention in recent years due to their high efficiency, suitability for renewable integration, and flexible control structure. In particular, photovoltaic (PV) systems combined with distributed energy storage units (DESUs) provide a promising platform for local energy generation and consumption [1–3]. However, managing the state-of-charge (SOC) balance among DESUs while maintaining DC bus voltage stability remains a major challenge, especially in decentralized and communication-limited environments.

In DC microgrids with multiple parallel energy storage units (ESUs), state-of-charge (SOC) imbalance is a critical issue that can severely compromise system performance and reliability. An unbalanced SOC distribution leads to disproportionate charging and discharging among ESUs, accelerating the degradation of certain battery modules while underutilizing others. This not only reduces the overall energy storage capacity and lifespan but also increases the likelihood of overcharge or deep discharge, potentially triggering protective shutdowns and compromising system availability. Furthermore, SOC imbalance can impair power-sharing accuracy, resulting in unstable bus voltage regulation and reduced microgrid resilience under fluctuating load or generation conditions [4]. Therefore, effective SOC balancing control is essential for maintaining both the operational safety and long-term economic viability of DC microgrids.

Over the past decade, various SOC balancing strategies have been developed to address the aforementioned challenges. Conventional approaches typically rely on droop control with SOC-dependent coefficients [5], allowing units with higher SOC to contribute more power during discharge and absorb less during charge, thereby promoting gradual equalization. Advanced methods extend this principle by integrating model predictive control, fuzzy logic-based adaptive droop, or distributed consensus algorithms, which enhance balancing speed and adaptability under dynamic operating conditions. Hardware-based solutions, such as active and passive balancing circuits, have also been explored to directly redistribute charge between modules. While these methods have demonstrated varying degrees of effectiveness, they often involve trade-offs between control complexity, convergence speed, and system scalability. Consequently, there remains a need for SOC balancing strategies that combine rapid convergence, robustness to operational uncertainties, and ease of integration into existing microgrid control frameworks.

A widely adopted approach for decentralized control in DC microgrids is the droop control strategy [6–8], which adjusts the output current of each storage converter based on a predefined voltage-current slope [9]. This method enables proportional load sharing without relying on centralized communication. However, conventional droop control neglects the SOC status of individual batteries [10], often resulting in SOC divergence, bus voltage deviations, and inefficient energy utilization. For example, fixed droop coefficients may cause energy-rich units to be underutilized and low-energy units to face overdischarge risks.

Recent studies have proposed advanced SOC balancing methods, such as fuzzy adaptive control, consensus-based control, MPC, and distributed optimization approaches. While these methods can achieve excellent balancing performance, they often involve higher computational complexity, communication requirements, or implementation costs. In contrast, the proposed method focuses on improving the conventional droop-control framework while preserving its decentralized structure and implementation simplicity. Many researchers have explored improved control strategies. Model Predictive Control (MPC)-based droop tuning [11] and voltage-compensated strategies [12] have demonstrated enhanced system responsiveness. More recently, AI-based approaches such as reinforcement learning, fuzzy logic, and neural networks have been applied to predict SOC, dynamically adjust droop coefficients, or optimize power sharing [13–15]. These data-driven methods show strong adaptability in nonlinear environments and uncertain conditions. In addition, Multi-Agent Systems (MAS) have gained traction for their capability to support distributed decision-making and coordination among multiple DESUs. MAS-based droop control frameworks enable decentralized cooperation through local agents, increasing system resilience and flexibility.

https://doi.org/10.3390/app16147358

Simulation results demonstrate that the average balancing time of the SOC has been reduced by 52.6% under the three different operating modes. Furthermore, this paper also demonstrates that the reduction in unbalanced time will potentially lead to a decrease in the cost of energy storage units.

The main contributions of this paper are summarized as follows:

(1) An improved SOC-based adaptive droop control strategy is proposed for DC microgrids, in which a nonlinear arctangent function is employed to enhance the sensitivity of droop coefficient adjustment under small SOC deviations, effectively accelerating SOC equalization.
(2) A capacity-aware compensation mechanism is incorporated into the droop coefficient design, enabling proportional power sharing among distributed energy storage units with heterogeneous capacities.
(3) An acceleration factor is introduced to further improve the SOC convergence speed without increasing control complexity or inducing excessive transient instability.
(4) The proposed control strategy is comprehensively evaluated through MATLAB/Simulink simulations under discharging, charging, and irradiance variation scenarios, demonstrating significant improvements in SOC balancing speed and overall dynamic response compared with conventional SOC-based droop control methods.
(5) A time-integrated SOC deviation perspective is introduced to discuss the potential impact of SOC imbalance duration on battery degradation accumulation and long-term economic performance of DC microgrids.

2. Traditional Droop Control Strategy

In this study, conventional droop control strategies are categorized into two types: those that do not consider SOC balancing and those that do. The traditional droop control strategy without SOC balancing achieves output current sharing among converters by adjusting the value of virtual resistance. However, due to constraints imposed by bus voltage regulation and current distribution, the virtual resistance must be selected within an appropriate range—it should be neither too large nor too small. On the other hand, traditional droop strategies that account for SOC balancing also face a dilemma in parameter tuning, as they struggle to simultaneously ensure system stability and improve the efficiency of SOC equalization.

2.1. Traditional Droop Control Strategy Without SOC Balancing Consideration

2.1.1. Strategy Without SOC Balancing Consideration Introduction

Since there is no reactive power flow in DC microgrids, the bus voltage can be directly used as a reference variable to maintain voltage stability [16–18]. A voltage–current dual-loop control strategy is adopted, in which the inner loop controls the current and the outer loop regulates the voltage [19]. The control block diagram is shown in Figure 1.

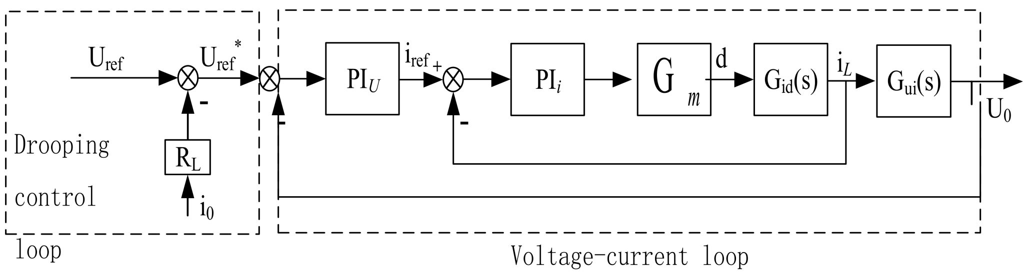

Figure 1. Traditional droop control chart.

The droop control method draws inspiration from the characteristics of conventional synchronous generators. By multiplying a predefined virtual resistance R_L with the output current i_o, a droop voltage U_{ref} signal is generated. This signal is then subtracted from the bus reference voltage to obtain an updated voltage reference U^*_{ref}. As shown in Figure 1, PI_U and PI_i represent the proportional–integral (PI) control coefficients for voltage and current loops, respectively. R_L denotes the virtual resistance. Since R_L is a virtual component, it does not cause actual power loss. In practical applications, adjusting the value of R_L allows for balanced current and power sharing among converters without requiring additional communication links [20]. The corresponding characteristic expression is given as follows:

$$U^*_{ref} = U_{ref} - i_o \cdot R_L \tag{1}$$

To present its drooping characteristic more intuitively, the floor plan is shown in Figure 2.

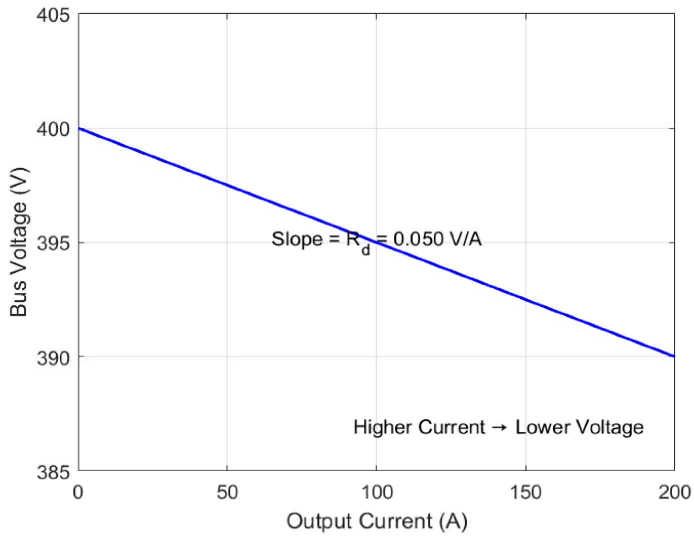

Figure 2. Voltage–current droop characteristic.

Next, this paper illustrates the topological principle that "equal distribution of converter output current and power can be achieved by adjusting only the R_L coefficient" through a specific example. The scenario is described as follows.

The circuit diagram for the case where two DESUs converters are connected in parallel is shown in Figure 3.

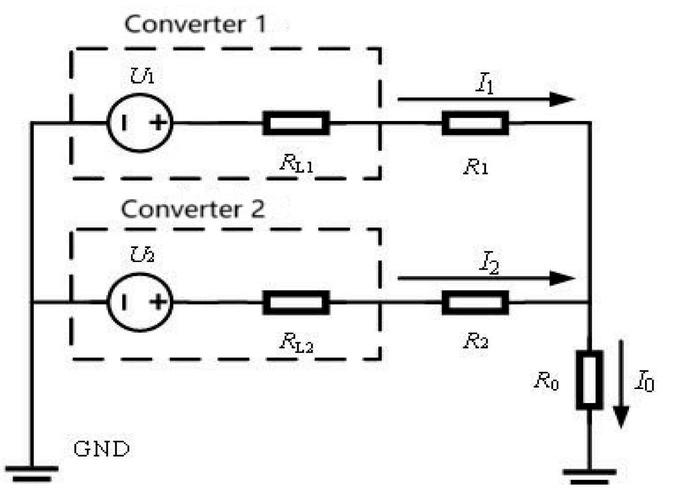

Figure 3. Parallel equivalent circuit diagram of the control converter.

In Figure 3, U_1 and U_2 represent the output voltages of the two DESUs converters, R_{L1} and R_{L2} are the virtual resistances of the converters, R_1 and R_2 denote the line impedances between the converters and the DC bus, and R_0 is the load resistance. Based on the equivalent circuit shown in Figure 3, the relationship between the converter output reference voltage and output current can be derived as follows [21]:

$$\begin{cases} U_1 - I_1(R_{L1} + R_1) - I_0 R_0 = 0 \\ U_2 - I_2(R_{L2} + R_2) - I_0 R_0 = 0 \end{cases} \tag{2}$$

In the equation, I_1 and I_2 represent the output currents of the converters.

From Equation (2), the current ratio between the two converters can be obtained as:

$$\frac{I_1}{I_2} = \frac{(R_{L2} + R_2 + R_0)U_1 - U_2 R_0}{(R_{L1} + R_1 + R_0)U_2 - U_1 R_0} \tag{3}$$

In DC microgrids, the line impedances R_1 and R_2 are typically much smaller than the predefined virtual resistances R_{L1} and R_{L2} due to the relatively short line distances. Therefore, when the output voltages of the distributed energy storage units (DESUs), U_1 and U_2, are equal, the current ratio between the converters can be approximately expressed as:

$$\frac{I_1}{I_2} = \frac{R_{L2}}{R_{Ll}} \tag{4}$$

From Equation (4), it can be concluded that, under the condition of equal output voltages among the distributed energy storage units (DESUs), the output current of the converters can be regulated by adjusting the values of the virtual resistances, thereby achieving current-sharing control.

In DC microgrids with DESUs of heterogeneous power ratings, proportional power sharing (rather than equal sharing) is often required to match converter capacities. As derived from Equation (4), the current ratio between two converters is inversely proportional to their droop coefficients. By intentionally setting R_{Li} values according to unit capacities (e.g., $R_{L1}/R_{L2} = C_2/C_1$), the proposed strategy naturally enables capacity-weighted power distribution while maintaining SOC balancing.

2.1.2. Strategy Without SOC Balancing Consideration Limitation

To minimize the influence of line impedance on current distribution, the virtual resistance is typically set to a relatively higher value. However, an excessively large virtual resistance may lead to a noticeable voltage drop on the DC bus. This voltage drop, denoted as ΔU, can be expressed as:

$$\Delta U = \left(R_L + R_{\mathrm{i}}\right) i_{\mathrm{o}} \tag{5}$$

The impact on voltage and current is illustrated in Figure 4.

As shown in Figure 4, when the virtual resistance is set to a relatively low value, the voltage drop ΔU on the DC bus remains small. However, the difference in output currents between converters ΔI_{12} becomes significant, preventing balanced current sharing [22]. Conversely, increasing the value of the virtual resistance helps to reduce the current deviation among modules, but it also aggravates the voltage drop $\Delta I_{12}{}^*$ on the DC bus, thereby compromising voltage stability.

Therefore, when selecting the droop coefficient, it is necessary to strike a balance between current sharing and voltage stability. Typically, to avoid excessive bus voltage drop, the virtual resistance should be set below the ΔU_{max} ratio of the maximum allowable bus voltage deviation to the output current i_{omax} Alternatively, a bus voltage compensation strategy can be employed for correction.

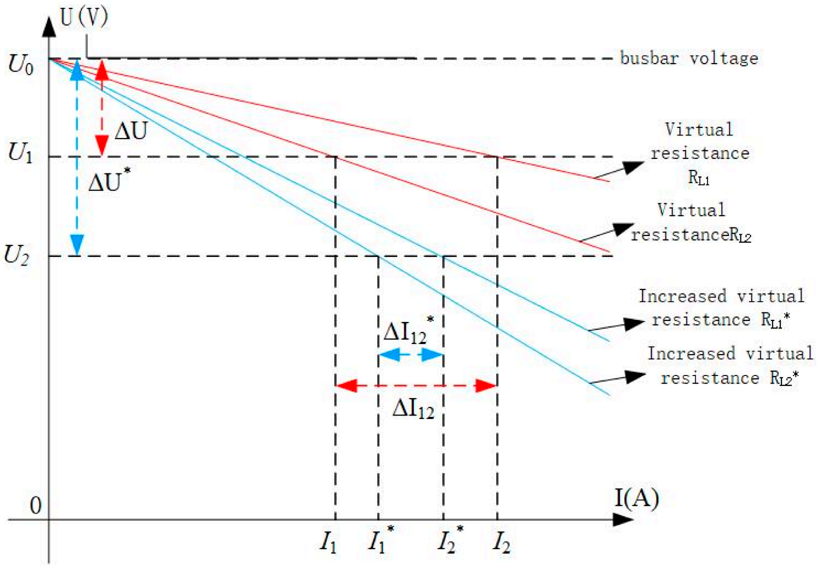

Figure 4. Voltage-current influence diagram.

However, in conventional droop control schemes, the virtual resistance is usually fixed and does not take into account the state of charge (SOC) of the battery. This limitation may lead to battery overdischarge, consequently reducing its service life. To address this issue, this paper proposes an optimized droop control strategy in which the droop coefficient is dynamically adjusted based on the real-time SOC status of the battery. This approach not only extends the battery lifespan but also ensures rational power distribution and stable operation of the DC microgrid.

2.2. Conventional Droop Control Strategies Considering SOC Balancing

2.2.1. Strategies Considering SOC Balancing Introduction

As analyzed above, the use of a constant virtual resistance in traditional droop control may result in battery overcharging or overdischarging, which shortens the battery lifespan and adversely affects the reliable operation of the power system.

The state of charge (SOC) of the battery is defined as shown in Equation (6):

$$SOC = \frac{Q}{C_i} \tag{6}$$

In the equation, Q is the rated charge capacity of the energy storage unit, and C_i is its rated energy capacity.

In DESUs, the SOC estimation of the battery is conducted using the Coulomb counting method, as described in the literature [23]. The calculation is given in Equation (7):

$$SOC_{it} = SOC_{i0} - \frac{1}{C_i}\int_0^t i_{ibat}dt \tag{7}$$

In the equation, SOC_{it} is the real-time state of charge of the energy storage unit, SOC_{i0} is the initial SOC value, i_{ibat} is the output current of the storage unit, and C_i is the capacity of the energy storage unit.

The output power of a DESU is given by:

$$P_{\mathrm{i}} = U_{\mathrm{ibat}} i_{\mathrm{ibat}} \tag{8}$$

In the formula: i_{ibat} is the output current of the energy storage unit; U_{ibat} is the output voltage of the energy storage unit is.

When two energy storage devices are connected in parallel, the SOC state formula is:

$$\begin{cases} \mathrm{SOC}_1 = \mathrm{SOC}_{10} - \frac{1}{C_1 U_{bat1}} \int p_1 dt \\ \mathrm{SOC}_2 = \mathrm{SOC}_{20} - \frac{1}{C_2 U_{bat2}} \int p_2 dt \end{cases} \tag{9}$$

The setting formula of the droop coefficient based on SOC equalization [24] is shown in Equation (10) as follows:

$$R(\mathrm{SOC}_i) = \begin{cases} k_0 \mathrm{SOC}^n, P_i < 0 \\ \frac{K_0}{\mathrm{SOC}_i^n}, P_i > 0 \end{cases} \tag{10}$$

In the formula: n is the exponential coefficient, and it is equal to 3 in the simulation of this paper; K_0 is the initial value of the sagging coefficient and it is equal to 2.5 during the simulation in this paper. In Equation (10), the coefficients k_0, K_0, and the exponent n jointly determine the adaptive slope of the SOC-based droop function. A larger n value accelerates SOC convergence but may induce transient current overshoot, whereas a smaller n provides smoother regulation at the cost of slower balancing speed [25]. The constants k_0 and K_0 are tuned to balance the responsiveness of power redistribution and voltage stability under both charging ($P_i < 0$) and discharging ($P_i > 0$) modes. The values adopted in the simulations were selected through preliminary trials to achieve a compromise between rapid SOC equalization and minimal voltage deviation.

In traditional SOC-based droop control methods, the droop coefficient is adjusted according to the current SOC value of the battery, enabling a certain degree of SOC balancing [26]. However, since the SOC variation during operation is relatively small, the corresponding adjustment range of the droop coefficient is limited, making it difficult to achieve rapid SOC equalization. Although increasing the exponential factor n can accelerate the balancing process, it may also lead to system instability [27].

2.2.2. Strategies Considering SOC Balancing Limitation

However, due to the relatively small variation range of the SOC during operation, the adjustment range of the droop coefficient is limited, making it difficult to achieve rapid SOC equalization. Although increasing the exponential factor n artificially can accelerate the balancing process, it may lead to a reduction in system stability [28]. Therefore, this paper proposes an improved design of the droop coefficient to enhance SOC equalization efficiency while preserving stable system operation under the studied conditions.

3. Improve SOC Equalization Control Strategy

To address the limitations of traditional SOC-based droop control methods—including slow convergence and insufficient adaptability—this section introduces a refined multi-layered droop coefficient framework [29]. The enhanced approach incorporates a nonlinear arctangent-based response, capacity compensation, an acceleration factor, and a protection mechanism. These components collectively form a dynamic and physically interpretable droop adjustment system.

3.1. Motivation and Overview

Conventional SOC-driven droop coefficients often exhibit limited sensitivity due to the small dynamic range of SOC during normal operation [30]. This restricts the controller's ability to equalize energy quickly [31]. To overcome this, the proposed method formulates a flexible droop coefficient adjustment using the arctangent function, which provides a smooth and nonlinear response to SOC deviations. Additionally, capacity discrepancies among energy storage units (ESUs) are considered by introducing a compensation term, and the system's responsiveness is further enhanced through an acceleration factor.

It should be emphasized that the proposed method is not intended to replace advanced control frameworks such as model predictive control (MPC), fuzzy-logic control, or consensus-based distributed control. Instead, the objective of this study is to improve the SOC balancing performance of conventional droop control while preserving its decentralized structure, low computational burden, and ease of implementation.

Compared with existing SOC-based droop strategies, the proposed approach enhances droop coefficient adaptability through an arctangent-based nonlinear adjustment mechanism, capacity-aware compensation, and an acceleration factor. These modifications improve SOC equalization speed without introducing additional communication requirements or complex optimization procedures.

3.2. Mathematical Formulation

The improved droop coefficient is calculated using:

$$R_{Li} = R_L + \alpha_i \cdot arctan[N_i \cdot (SOC_i - SOC_0)] \tag{11}$$

In the formula: R_L is base droop resistance; α_i is capacity compensation factor; N_i is Acceleration factor (nonlinear gain); SOC_i is real-time state of charge of unit; SOC_0 is reference SOC (typically system average).

The compensation and acceleration terms are defined as:

$$\alpha_i = K_\alpha \cdot \frac{C_i}{C_{max}} \tag{12}$$

$$N_i = K_N \cdot |SOC_i - SOC_0| \tag{13}$$

In the formula: C_i is capacity of unit; C_{max} is maximum capacity among all ESUs; K_α, K_N are design constants (set to 1 and 3 respectively in simulation).

When $SOC_i = SOC_0$, the deviation vanishes, the droop coefficient returns to its default initial value R_L, the gain term reduces to zero, and no additional modulation is imposed on the droop characteristics. At this point, the droop characteristic can be expressed as:

$$U^*_{\mathrm{ref}} = U_{\mathrm{ref}} - i_{\mathrm{ibat}} R(SoC_i) \tag{14}$$

To ensure a fair comparison, both the traditional and proposed droop control strategies are implemented using the same exponential gain parameter n = 3.

The parameters K_α, K_N, n, and R_L adopted in this study were selected through preliminary simulation trials to achieve a compromise between SOC balancing speed, voltage regulation performance, and operational stability. In particular, excessively large values of K_N and n may accelerate SOC convergence but could increase transient current fluctuations, whereas excessively small values may lead to slower balancing performance. Therefore, the selected parameter set represents a practical engineering trade-off under the considered operating conditions.

It should be noted that the parameter values reported in this paper are not intended to represent universally optimal settings for all DC microgrid configurations. Their optimal selection may depend on system topology, storage capacity, converter ratings, and operating conditions. A comprehensive parameter sensitivity analysis and optimization study will be considered in future work.

https://doi.org/10.3390/app16147358

3.3. Physical Interpretation and Component Summary

The summary of the functions of each component in the improvement method is shown in Table 1.

Table 1. Functional Roles of Components in the Multi-Layered Droop Control Design.

Component	Role
Arctangent Function	Enables smooth, nonlinear adaptation of R_{Li} to SOC deviation.
Capacity Compensation ($\boldsymbol{\alpha_i}$)	Ensures power distribution is proportional to ESU capacity.
Acceleration Factor ($\boldsymbol{N_i}$)	Amplifies droop sensitivity for faster SOC balancing.
Base Resistance ($\boldsymbol{R_L}$)	Default droop value when no deviation is present.

Flexible Response Module (Arctangent): Smooth transition helps mitigate abrupt droop coefficient variations and contributes to stable operating behavior. When $SOC_i > SOC_0$, R_{Li} increases (during charging), discouraging further energy intake. When $SOC_i < SOC_0$, R_{Li} decreases (during discharging), encouraging more contribution. Compared to the exponential SOC control in Equation (10), the arctangent-based function in Equation (11) offers a broader linear operating range and smoother response, allowing the controller to avoid saturation while maintaining fast and stable SOC balancing.

Capacity Compensation Module: Adjusts R_{Li} proportionally to the relative capacity of each unit, enabling fair energy allocation and preventing overburdening smaller units.

Acceleration Factor: Increases responsiveness to large SOC imbalances, improving convergence without aggressive gain settings.

It should be noted that the primary objective of the proposed strategy is to accelerate SOC equalization through adaptive droop coefficient adjustment. The arctangent function was intentionally selected because of its continuous and bounded characteristics, which prevent abrupt parameter changes that may adversely affect converter operation. In addition, the proposed control law preserves the conventional droop-control structure and only modifies the droop coefficient adaptively according to SOC deviation. Therefore, the strategy does not introduce additional feedback loops or high-order dynamic components that could significantly alter the original system dynamics. Additional system-level simulation results are provided in Section 4.4 to evaluate the influence of the proposed strategy on overall DC microgrid operation.

The arctangent function was selected due to its continuous, bounded, and smoothly varying nonlinear characteristics. Compared with exponential-based adaptive droop methods, the arctangent function provides a more gradual transition when the SOC difference becomes large, thereby reducing the risk of excessively aggressive parameter variations. Compared with fuzzy-logic-based approaches, the proposed method does not require rule-base design, membership function tuning, or extensive parameter adjustment, resulting in a simpler implementation with lower computational complexity. Furthermore, the bounded output characteristic of the arctangent function naturally limits the variation range of the adaptive droop coefficient, which is beneficial for maintaining smooth control behavior throughout the SOC equalization process.

As shown in Table 2, existing adaptive SOC balancing strategies mainly focus on improving equalization speed through nonlinear droop adjustment or intelligent control techniques. However, many methods either increase implementation complexity or lack consideration of the long-term economic impact associated with SOC imbalance. The proposed approach combines a bounded arctangent-based adaptive droop mechanism with an economic-performance-oriented evaluation framework, providing a balance between control effectiveness, implementation simplicity, and lifecycle sustainability. Table 2 presents a

https://doi.org/10.3390/app16147358

qualitative comparison based on the simulation results obtained in this study. The evaluation criteria are defined according to key performance indicators, including SOC balancing speed, voltage stability, and current sharing performance.

Table 2. Comparison of representative SOC balancing control methods.

Method	Adaptive Capability	Computational Complexity	Parameter Tuning	Output Boundedness	Economic Consideration
Fixed droop control	Low	Low	Simple	Yes	No
Exponential droop control	Medium	Low	Moderate	No	No
Fuzzy adaptive control	High	High	Complex	Depends on design	No
Neural-network-based control	High	Very high	Complex	Depends on training	No
Proposed arctangent adaptive droop	High	Low	Simple	Yes	Yes

3.4. Protection Mechanism

To ensure operational safety, a threshold-based cutoff mechanism is employed. If it exceeds upper/lower bounds, the unit is temporarily removed from service. This prevents overcharge/discharge conditions.

According to Figure 5, the SOC values of all DESUs were constrained within the predefined safety range of 10–90% throughout the simulation. These results quantitatively verify the effectiveness of the proposed protection mechanism.

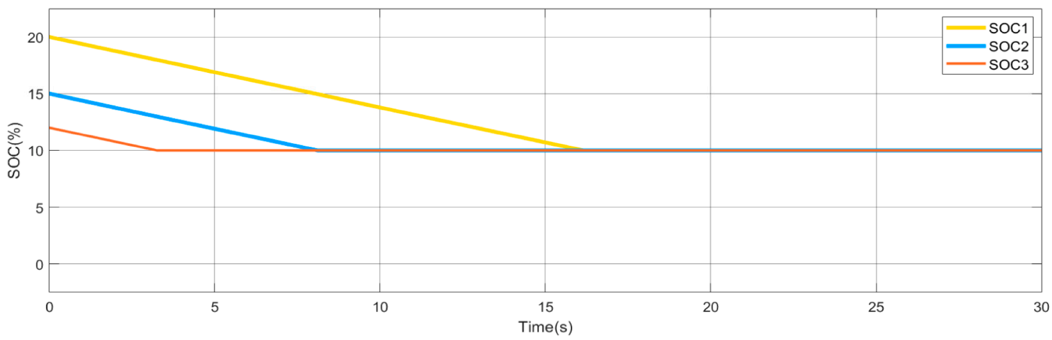

Figure 5. Performance of the Protection Mechanism During Simulation.

3.5. Algorithm Flow

To clarify the implementation logic of the proposed control strategy, a flowchart is provided in Figure 6, which illustrates the sequential process of calculating the adaptive droop coefficient based on real-time SOC values. The strategy integrates a nonlinear arctangent-based adjustment, capacity-aware compensation, and an acceleration factor to dynamically reshape the droop behavior according to the system state. Additionally, a protection mechanism is embedded to prevent overcharge or overdischarge conditions by enforcing SOC thresholds. This multi-layered structure enables responsive and safe coordination among distributed energy storage units in DC microgrids.

It should be noted that the proposed method preserves the conventional droop-control framework and only adaptively modifies the droop coefficient according to the SOC deviation. The adopted arctangent function is continuous and bounded, which prevents abrupt coefficient variations and helps ensure smooth control action. Furthermore, no additional feedback loops or higher-order dynamic components are introduced into the original control structure. Therefore, the proposed strategy mainly affects the transient equalization process while retaining the fundamental operating characteristics of conventional droop control.

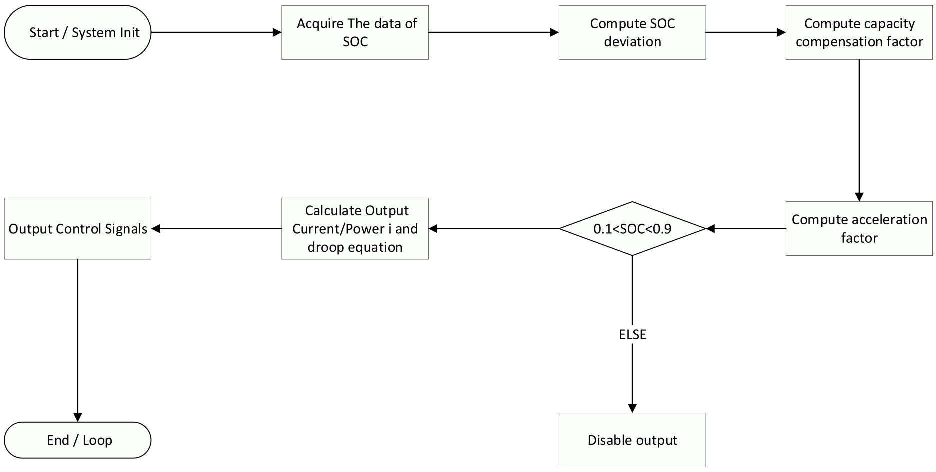

Figure 6. Control flow of the proposed SOC-based adaptive droop strategy.

4. Analyze the System Simulation

To verify the effectiveness of the proposed SOC-balancing-based improved droop control strategy, a photovoltaic DC microgrid simulation platform was developed using Simulink. The simulation system comprises three parallel energy storage subsystems (ESS1, ESS2 and ESS3), a photovoltaic generation system (PV), and a DC load. The energy storage subsystems are connected to the common DC bus through bidirectional DC/DC converters, and voltage droop control is employed to achieve power distribution and energy management.

The PV generation module incorporates a variable irradiance model to evaluate the system's adaptability under dynamic environmental conditions. All control strategies, including the conventional droop control and the proposed adaptive improved droop control, are implemented via discrete controllers with a control cycle of 1 ms.

During the simulation, system performance was tested under three scenarios: discharging, charging, and irradiance variation. These tests were designed to comprehensively evaluate the proposed strategy's effectiveness in improving SOC equalization speed under various operating conditions.

To facilitate understanding of the proposed control strategy, a simplified control block diagram is provided in Figure 7. The diagram illustrates the main signal flow and key components of the proposed adaptive droop mechanism, including the SOC deviation calculation, arctangent-based nonlinear adjustment, capacity compensation factor, acceleration factor, and droop coefficient generation process. Compared with the detailed Simulink implementation model, the simplified block diagram more clearly highlights the control logic and the contribution of each functional module.

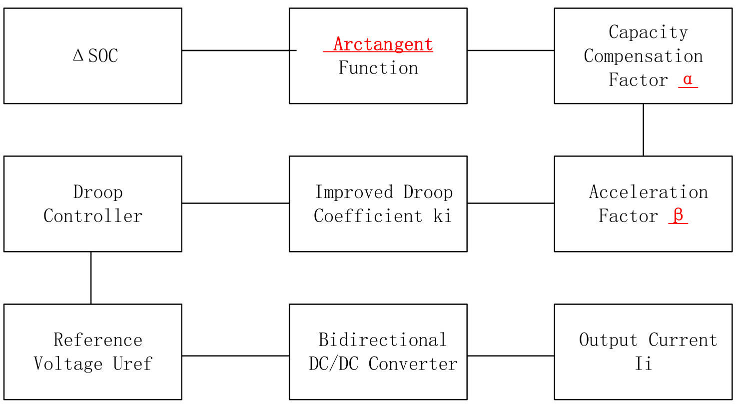

Figure 7. Control structure of the proposed SOC-adaptive droop strategy.

Specific simulation parameters are set as follows: The reference value for the DC bus voltage is $U^*_{\mathrm{ref}} = 400$ V. In the simulation model, the port voltage of each battery unit is set to 200 V with a capacity of 2 Ah. The connected load is purely resistive with a resistance of 5 Ω. The maximum and minimum state of charge (SOC) of the energy storage units are set to 90% and 10%, respectively. The internal resistance of the battery is set to 1 Ω. In the voltage compensation control loop, the proportional and integral gains of the PI controller are $k_{\mathrm{p}} = 2$ and $k_{\mathrm{i}} = 30$, and the filter inductance L is set to 5 mH.

In the Boost converter section, the circuit component parameters are set as follows: the photovoltaic side filter capacitor C_{pv} = 10, boost inductor L = 0.06 and output side filter capacitor C = 20 mF. For the control system, the parameters of the voltage loop PI controller are $k_{\mathrm{pu}} = 1$ and $k_{\mathrm{iu}} = 20$, while the integral gains of the current loop PI controller are $k_{\mathrm{pi}} = 1$ and $k_{\mathrm{ii}} = 1$.

4.1. Single-Operating-State Control Strategy

4.1.1. Simulation Analysis of Control Strategy in Discharge Mode

To evaluate the effectiveness of the proposed improved droop control strategy in enhancing SOC balancing during the discharging mode, a constant-load discharging simulation was conducted.

In this test, the system was subjected to a constant power load, while the solar irradiance was kept unchanged throughout the discharge process to isolate the effects of external disturbances.

The performance of the proposed strategy was compared with that of the conventional droop control by analyzing the evolution curves of the SOC in each energy storage unit. These comparisons aimed to assess the proposed method's advantages in promoting dynamic energy equalization.

In the discharging mode, the maximum output power of the photovoltaic system is set to 15 kW. The initial state of charge (SOC) of the three energy storage units is set as follows: $SoC_1 = 63\%$, $SoC_2 = 60\%$, and $SoC_3 = 57\%$. During the simulation, the line resistance is uniformly set to 0.01 Ω. For the traditional droop control strategy, the droop coefficients of the three energy storage units are all set to 0.5 as a baseline for comparison.

SOC Evolution in Discharge Mode

As shown in Figure 8, the traditional droop control strategy, with a fixed droop coefficient, cannot dynamically adjust based on the state of charge (SOC) of the energy storage units, making it difficult to achieve SOC balance between different DESUs. As seen in Figure 8a, the three DESUs only gradually reach SOC equality after 47.5 s of simulation. In contrast, the improved control strategy introduces the arctanx function and overlays the droop amplification coefficient, allowing the droop coefficient to respond more sensitively to SOC variations. In Figure 8b, it can be observed that the three energy storage units achieve SOC equilibrium within 25 s. The optimized control method has shortened the balancing time by 47.4%.

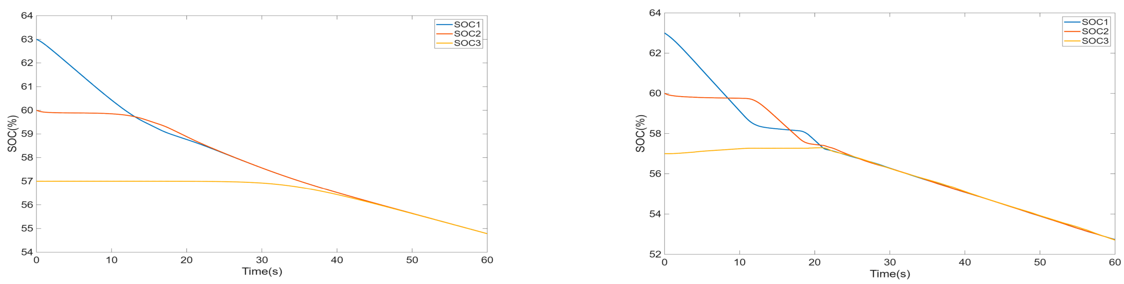

(**a**) Carry out the control scheme before improvement (**b**) Carry out the improved control scheme

Figure 8. Comparison chart of the SOC status of energy storage units before and after improvement.

4.1.2. Simulation Analysis of Control Strategy in Charging Mode

To further validate the adaptability and performance advantages of the proposed improved droop control strategy under charging conditions, a simulation was conducted under constant irradiance.

In this scenario, a stable-output photovoltaic array is connected to the system, and under low load demand, the excess energy is preferentially stored in the energy storage units.

By comparing the SOC evolution trends during the charging process under both the conventional droop control and the proposed strategy, the effectiveness of the proposed method in accelerating SOC equalization is comprehensively evaluated.

In charging mode, the maximum output power of the photovoltaic modules is set to 20 kW. The initial state of charge (SOC) of the three energy storage units (DESUs) is set as follows: $SoC_1 = 18\%$; $SoC_2 = 17\%$; $SoC_3 = 16\%$. During the simulation, the line resistance is uniformly set to 0.01 Ω. For the traditional droop control strategy, the droop coefficients of the three energy storage units are all set to 1 as a baseline comparison condition.

SOC Evolution in Charging Mode

Figure 9 shows the comparison of the SOC variations in three energy storage units (DESUs) under two different droop control strategies in charging mode.

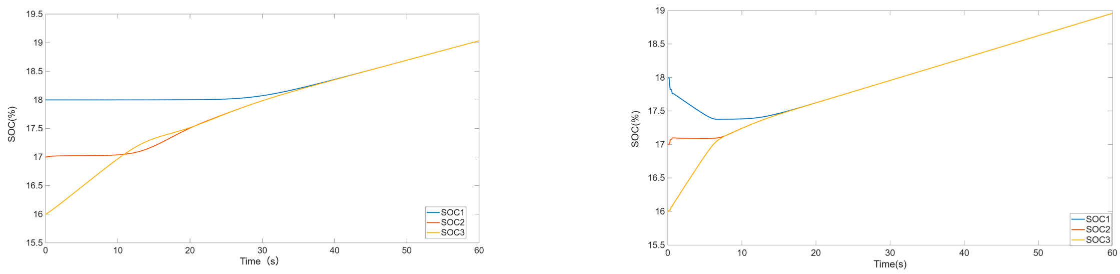

(**a**) Carry out the control scheme before improvement (**b**) Carry out the improved control scheme

Figure 9. A comparison chart of the SOC status of the energy storage unit before and after improvement in charging mode.

Figure 9a shows the pre-improvement SOC-based droop control scheme. Although this strategy can achieve SOC balance for the three energy storage units, the balancing speed is relatively slow since no acceleration mechanism was introduced. The SOC balance is only achieved around 38 s.

In Figure 9b, the improved control scheme introduces a nonlinear function and a droop amplification factor, significantly enhancing the balancing efficiency. The three energy storage units reach an identical SOC state in about 18.5 s. Compared to the pre-improvement scheme, the optimized control method has shortened the balancing time by 51.3%, confirming the effectiveness of the strategy in improving charging efficiency and system dynamic response.

4.2. Multi-Scenario Adaptive Control Strategy

To assess the adaptability and robustness of the proposed improved droop control strategy under dynamic external conditions, a simulation was conducted with varying solar irradiance.

In this test, step changes in irradiance were introduced to emulate real-world fluctuations in solar radiation and their impact on system operation.

By comparing the SOC variation curves of the energy storage units under both the conventional droop control and the proposed strategy, the effectiveness of the proposed method in maintaining energy balance in the presence of irradiance disturbances is verified and analyzed.

In the practical application scenario of a photovoltaic-storage hybrid DC microgrid, due to the fluctuations in sunlight intensity, the output power of the photovoltaic generation often varies. To verify the operation performance of the energy storage system under changing sunlight conditions, this study conducted a simulation analysis, focusing on the effectiveness of the Distributed Energy Storage Units (DESUs) in balancing the battery state of charge (SOC) during continuous charging and discharging. Specifically, during the operation, the photovoltaic module is in the discharging stage from 0 to 20 s, with a maximum output power of 15 kW. At 20 s, the output power suddenly drops to 10 kW and remains stable at this level until 40 s. From 40 s onwards, the photovoltaic module enters the charging state, with the output power increasing to 20 kW and maintaining this level until the end of the simulation. Under this control strategy, DESUs discharge from 0 to 20 s and gradually reach the SOC equilibrium. After 40 s, when the photovoltaic output increases, DESUs switch to a stable charging mode. The initial working state of charge for the three energy storage units is set as follows: $SoC_1 = 44\%$; $SoC_2 = 42\%$; $SoC_3 = 40\%$.

SOC Evolution in Multi-Scenario

From Figure 10a, it can be observed that with the original control strategy, the system achieves SOC equilibrium at 39 s. When the photovoltaic output power suddenly increases to 20 kW at 40 s, the energy storage system begins to enter the charging state. In contrast, Figure 10b shows the results obtained using the optimized control strategy: the three distributed energy storage units (DESUs) achieve preliminary SOC convergence at 16 s. By 20 s, when the photovoltaic output drops from 14 kW to 10 kW, the energy storage system accelerates discharging and maintains a relatively stable operation. By 40 s, the SOC of the three storage units is fully balanced. Subsequently, as the photovoltaic output increases, the system enters the rapid charging phase. Compared to the original strategy, the optimized control method has shortened the balancing time by 59%.

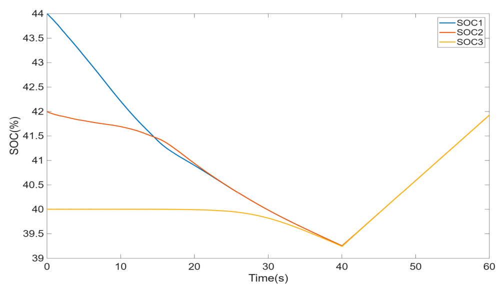

(**a**) Carry out the control scheme before improvement

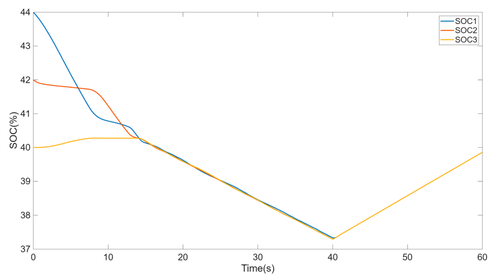

(**b**) Carry out the improved control scheme

Figure 10. A comparison chart of the SOC status of the energy storage unit before and after improvement in Multi-Scenario.

4.3. Economic Perspective Analysis

In conventional studies of SOC balancing control for DC microgrids, the evaluation criteria are mainly focused on dynamic indicators such as balancing speed, voltage recovery time, and transient stability [32–34]. However, the long-term economic impact caused by prolonged SOC imbalance among distributed energy storage units (DESUs) is often neglected.

In practical engineering systems, sustained SOC imbalance may lead to uneven charge/discharge stress among battery units, resulting in accelerated local degradation, inconsistent aging, and reduced effective lifetime of the energy storage system [35]. Consequently, reducing the duration of SOC imbalance is not only beneficial for dynamic control performance but also important for potentially lowering lifecycle operating costs. It should be noted that the following analysis is intended to provide a simplified qualitative framework for illustrating the potential relationship between SOC imbalance duration and long-term battery utilization efficiency. The model does not attempt to comprehensively represent all battery aging mechanisms and should not be interpreted as a rigorous lifetime prediction model.

To quantitatively evaluate the cumulative influence of SOC imbalance, a time-integrated SOC deviation index is introduced as follows:

$$J_{SOC} = \int_0^T \sum_{i=1}^{n} |SOC_i - SOC_{avg}| dt \tag{15}$$

SOC_i represents the real-time state of charge of the ith energy storage unit, SOC_{avg} denotes the average SOC of the system, and T is the total operating duration.

The proposed indicator reflects the cumulative imbalance degree experienced by the energy storage system during operation. A larger J_{SOC} value indicates either a larger SOC deviation or a longer imbalance duration, both of which contribute to intensified battery degradation.

Considering that battery aging is closely associated with long-term unequal charging/discharging stress [36], the cumulative degradation factor can be approximately expressed as:

$$D = k \cdot J_{SOC} \tag{16}$$

where D is the cumulative degradation level and k is the degradation coefficient associated with battery characteristics.

Based on the cumulative damage concept, the effective lifetime of the battery system can be estimated as:

$$L = L_0 - D \tag{17}$$

where L_0 is the theoretical lifetime under ideal balanced operation conditions and L is the actual effective lifetime under practical operating conditions.

Accordingly, the battery replacement cost during the system lifecycle can be approximately described by:

$$C_{rep} = \frac{C_b}{L} \tag{18}$$

where C_b is the investment cost of the battery system and C_{rep} represents the equivalent replacement cost per operating cycle or unit time.

From the above relationship, it can be observed that reducing the SOC imbalance duration effectively decreases J_{SOC}, thereby mitigating cumulative degradation and contributing to improved battery utilization. As a result, the long-term replacement and maintenance costs of the energy storage system can be potentially reduced. Battery degradation in practical energy storage systems is affected by multiple factors, including temperature, depth of discharge, charge/discharge rate, cycle number, and calendar aging. Therefore, the proposed indicators are intended to reflect the relative influence of SOC imbalance duration rather than provide quantitative predictions of battery lifetime or replacement cost.

The simulation results presented in Sections 4.1 and 4.2 demonstrate that the proposed control strategy significantly shortens the SOC equalization time under different operating conditions. Specifically, the balancing time is reduced from 47.5 s to 25 s in discharging mode, from 38 s to 18.5 s in charging mode, and from 39 s to 16 s under irradiance variation conditions. The reduction ratios reach 47.4%, 51.3%, and 59%, respectively.

To provide a quantitative illustration of the economic-performance indicators introduced in Equation (15), Table 3 calculates J_{SOC} for each of the various working conditions. The values of the cumulative SOC imbalance index J_{SOC} reported in Table 3 are calculated according to (15) based on the simulation data. The numerical integration is performed using the recorded SOC values over the entire simulation interval with a sampling time of

0.0001 s. The resulting index reflects the accumulated SOC deviation among energy storage units over time and is expressed in a dimensionless form.

Table 3. Comparison of J_{SOC}.

Operating Mode	Conventional	Proposed	Reduction
Discharging	104.61	45.08	56.9%
Charging	30.55	8.66	71.6%
Irradiance variation	59.60	27.63	53.6%

Table 3 indicates that the proposed control strategy significantly reduces J_{SOC} compared with the conventional SOC-based droop control strategy. Specifically, J_{SOC} is reduced by 56.9%, 71.6%, and 53.6% under discharging, charging, and irradiance variation conditions, respectively.

According to Equations (16) and (17), the reduction of J_{SOC} contributes to mitigating degradation accumulation and improving the effective utilization of battery assets. Although the proposed analysis does not constitute a rigorous battery lifetime prediction model, these quantitative results provide further evidence that accelerating SOC equalization may offer potential economic benefits in long-term DC microgrid operation.

These improvements indicate that the DESUs remain in an imbalanced operating state for a substantially shorter duration, which directly reduces the cumulative SOC deviation index J_{SOC}. Consequently, the proposed strategy contributes not only to enhanced dynamic performance but also to reduced battery degradation accumulation and improved economic efficiency throughout the lifecycle of the DC microgrid.

Therefore, compared with traditional SOC-based droop control strategies, the proposed method provides a more economically sustainable solution for distributed energy storage coordination, offering potential benefits in battery replacement cost reduction and long-term system asset management.

4.4. Discussion on Overall DC Microgrid Operation

Although the primary objective of the proposed strategy is to improve SOC equalization performance among distributed energy storage units (DESUs), its influence on the overall operation of the DC microgrid should also be evaluated. Since the proposed method adaptively modifies the droop coefficient according to the SOC deviation, it is important to verify that this modification does not adversely affect system-level operating characteristics.

To investigate the impact of the proposed control strategy on DC microgrid operation, the DC bus voltage response was further analyzed in Charging Mode. The corresponding simulation result is shown in Figure 11.

As illustrated in Figure 11, the DC bus voltage fluctuates within approximately $\pm 0.75\%$ of the nominal value, which demonstrates that the proposed strategy maintains acceptable voltage regulation performance. The voltage deviation remains within an acceptable range during both charging and discharging transitions, indicating that the proposed SOC-adaptive droop control strategy preserves satisfactory voltage regulation performance while improving SOC equalization efficiency.

Moreover, the load current remains smooth without significant fluctuations, reflecting stable system operation. The PV output follows its expected generation profile and is not adversely affected by the proposed method. Meanwhile, the output currents of the storage units exhibit coordinated and smooth dynamic responses, which contribute to both effective SOC balancing and reliable system performance.

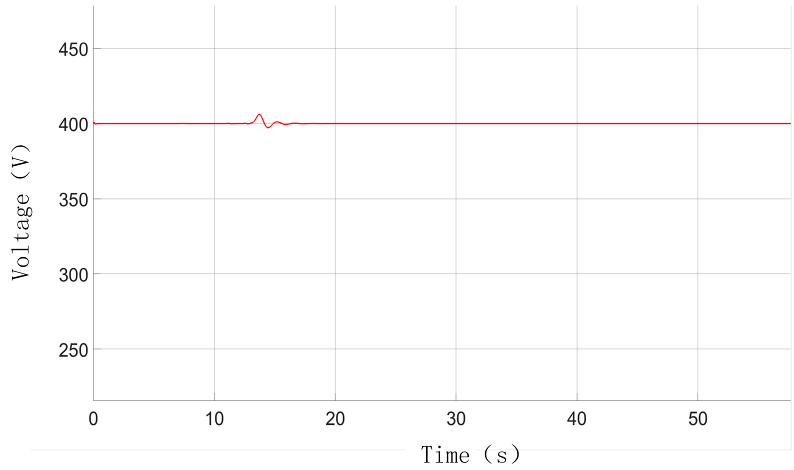

Figure 11. DC bus voltage curve graph.

The reason for this behavior is that the proposed method retains the conventional droop-control framework and only adaptively adjusts the droop coefficient according to the SOC deviation. Therefore, the fundamental operating characteristics of the original DC microgrid control system remain unchanged. These results suggest that the proposed strategy can improve SOC balancing performance without causing noticeable degradation of the overall operating performance of the DC microgrid under the considered operating conditions.

4.5. Practical Implementation Considerations

Although the present study focuses on simulation-based verification, the proposed control strategy is suitable for practical implementation in DC microgrid controllers. The algorithm mainly consists of SOC acquisition, arctangent function evaluation, and adaptive droop coefficient updating, which involve relatively simple arithmetic operations and do not require iterative optimization procedures or complex intelligent-control algorithms. Therefore, the computational burden is low and can be readily accommodated by commonly used digital control platforms such as DSPs and microcontrollers.

It is worth noting that oscillatory behavior (similar to hunting) may occur when the SOC difference between energy storage units exceeds approximately 2%. This phenomenon is mainly caused by the dynamic interaction between the adaptive droop coefficient adjustment and the SOC balancing mechanism.

Specifically, when the SOC deviation becomes relatively large, the proposed control strategy increases the regulation effort to accelerate SOC equalization. This may lead to temporary oscillations in current and voltage responses due to the closed-loop feedback dynamics.

However, these oscillations are bounded and gradually damped over time, and therefore do not affect the overall stability of the DC microgrid. In practical operation, such behavior can be mitigated by properly tuning the droop coefficients or introducing damping factors.

It should also be noted that the current study focuses on typical operating conditions, and extreme cases with large SOC differences or rapidly varying loads have not been exhaustively investigated. Further studies will consider a more comprehensive evaluation under diverse operating scenarios.

Furthermore, the proposed method preserves the conventional droop-control structure and only modifies the droop coefficient adaptively according to SOC deviation. Consequently, no additional communication infrastructure or specialized hardware is required. Since the arctangent function is continuous and bounded, moderate SOC estimation errors or measurement noise are not expected to cause abrupt coefficient variations. Nevertheless, a detailed investigation of hardware implementation issues, measurement uncertainty, and real-time experimental validation will be considered in future work.

5. Conclusions

This paper proposes an improved SOC-based adaptive droop control strategy for photovoltaic DC microgrids with distributed energy storage units (DESUs), aiming to address the limitations of conventional droop control methods in terms of slow SOC equalization. By introducing a nonlinear arctangent-based droop adjustment mechanism, a capacity compensation factor, and an acceleration term, the proposed strategy enhances the flexibility of droop coefficient regulation while maintaining satisfactory performance under the considered operating scenarios.

The effectiveness of the proposed strategy has been verified through MATLAB/Simulink simulations under discharging, charging, and irradiance variation scenarios. Compared with the conventional SOC-based droop control strategy, the proposed method improves SOC balancing performance. Specifically, the SOC equalization time is reduced from 47.5 s to 25 s in discharging mode, from 38 s to 18.5 s in charging mode, and from 39 s to 16 s under irradiance variation conditions. These results indicate faster SOC convergence and improved dynamic response within the scope of the considered simulation conditions.

In addition, a time-integrated SOC deviation index is introduced to evaluate the cumulative SOC imbalance during system operation. This index provides a useful performance metric for comparing SOC balancing effectiveness among different control strategies. It should be noted that this index is used for performance evaluation only and does not directly quantify battery degradation or lifetime in the absence of a validated aging model.

It should also be emphasized that the validation in this study is limited to the considered simulation scenarios. Broader operating conditions, such as a wider range of initial SOC distributions, load variations, and renewable energy fluctuations, have not been exhaustively investigated and require further study.

Future work will focus on extending the validation of the proposed strategy under more diverse operating conditions to further assess its robustness and practical applicability.

Overall, the proposed method improves SOC coordination performance under the considered simulation conditions and provides a feasible control approach for distributed energy storage management in DC microgrids.

Author Contributions: Conceptualization, Q.W., L.L. and J.G.; Methodology, S.W. and Q.W.; Software, X.W., C.Y., L.L. and W.L.; Validation, Z.W.; Formal analysis, X.W.; Investigation, X.W., S.W., Q.W. and Z.W.; Resources, C.Y., Q.W., L.L. and J.G.; Data curation, S.W. and Z.W.; Writing—original draft, X.W. and S.W.; Writing—review & editing, C.Y., J.G. and W.L.; Visualization, X.W.; Supervision, L.L., J.G. and W.L.; Project administration, W.L.; Funding acquisition, W.L. All authors have read and agreed to the published version of the manuscript.

Funding: National Key Research and Development Program Project (2021YFB1600202), Henan Transportation Investment Group Co., Ltd. Technology Project (HNJT2024-35).

Data Availability Statement: The data that support the findings of this study are available from the corresponding author upon reasonable request.

Conflicts of Interest: Authors Mr. Zhigang Wei and Mr. Linyi Li was employed by the company China Northwest Architectural Design and Research Institute Co., Ltd. and State Grid Xinjiang Electric Power Research Institute. The remaining authors declare that the research was conducted in the absence of any commercial or financial relationships that could be construed as a potential conflict of interest.

References

1. Zhang, L.; Yan, K.; Leng, X.; Lü, L.; Cai, G. Research on coordinated control strategy of independent DC microgrid based on SOC droop control. *Power Syst. Prot. Control* **2021**, *49*, 87–97. [CrossRef]
2. Yang, M.; Deng, S.; Zhao, Z. Coordinated operation of photovoltaic power generation system and energy storage device. *Energy Storage Sci. Technol.* **2025**, *14*, 3920–3922. [CrossRef]

3. Pang, J.; Sun, J. Discussion on application and economic benefits of distributed energy storage systems based on energy interconnection. *Energy Storage Sci. Technol.* **2025**, *14*, 868–870. [CrossRef]
4. Li, F.; Chang, T.; Li, H.; He, P.; He, W.; Huang, Z.; Wang, J. Pinning-based switching control for SOC balancing of supercapacitors: A switched system approach. *J. Energy Storage* **2025**, *109*, 115077. [CrossRef]
5. Guo, L.; Liu, X.; Li, X.; Wang, R.; Ren, H.; Wang, Z.; Sun, Q. A novel adaptive droop-based SoC balancing control strategy for distributed energy storage system in DC microgrid. *Int. J. Electr. Power Energy Syst.* **2025**, *165*, 110514. [CrossRef]
6. Lu, Z.; Miao, Z.; Cai, Y. A multi-energy storage SOC stable and balanced control strategy considering time-varying line impedance. *High Volt. Eng.* **2024**, *50*, 127–137. [CrossRef]
7. Yin, C.; Wang, D.; Liu, B.; Zhang, Q.; Gao, J.; Zhao, J. SOC balancing control strategy of DC microgrid based on voltage compensation. *Distrib. Util.* **2025**, *42*, 34–42. [CrossRef]
8. Wu, X.; Yang, Y.; Bai, Z.; Guo, H.; Guo, G.; Zhang, J. Research on SOC balancing droop control strategy for distributed energy storage units in islanded DC microgrid. *Energy Storage Sci. Technol.* **2025**, *14*, 3160–3169. [CrossRef]
9. Ren, X.; Li, T.; Ma, J.; Huang, Y.; Zhang, D.; Wu, Y. Optimal Capacity Configuration of Hybrid Energy Storage for Photovoltaic Microgrid Considering Charge State. *Electr. Meas. Instrum.* **2024**, *61*, 150–156. [CrossRef]
10. Kesavan, P.K.; Subramaniam, U.; Almakhles, D.J. Laboratory implementation of direct torque controller based speed loop pseudo derivative feedforward controller for PMSM drive. *CES Trans. Electr. Mach. Syst.* **2024**, *8*, 12–21. [CrossRef]
11. Zhu, Y.; Li, W.; Wu, H.; Ma, X.; Xu, D. Grid-connected power control and SOC balancing strategy for lithium battery energy storage systems. *Zhejiang Electr. Power* **2025**, *44*, 90–99. [CrossRef]
12. Hu, Y.; Zhou, R.; Huang, T.; Zhang, Y.; Ning, T.; Yu, J. SOC balancing strategy for grid-connected cascaded energy storage systems based on improved droop control. *Power Syst. Prot. Control* **2021**, *49*, 120–129. [CrossRef]
13. Peksen, M.; Spliethoff, H. Optimising pre-reforming for quality r-SOC syngas preparation using artificial intelligence (AI) based machine learning (ML). *Int. J. Hydrogen Energy* **2023**, *48*, 24002–24017. [CrossRef]
14. Sorouri, H.; Oshnoei, A.; Che, Y.; Teodorescu, R. A comprehensive review of hybrid battery state of charge estimation: Exploring physics-aware AI-based approaches. *J. Energy Storage* **2024**, *100*, 113604. [CrossRef]
15. DeSantis, C.; Hussein, A.R. AI SOC-based accelerator for speech classification. *IEEE Can. J. Electr. Comput. Eng.* **2022**, *45*, 222–231. [CrossRef]
16. Yang, F.; Liu, S.; Li, D. Finite control set model predictive control method of energy storage bidirectional DC-DC converter with mode activation. *Water Resour. Power* **2019**, *37*, 185–188. [CrossRef]
17. Ji, Y.; Wang, D.; Wu, H.; Wu, M.; Lü, Q. Active damping method for improving the stability of DC microgrid. *Trans. China Electrotech. Soc.* **2018**, *33*, 370–379. [CrossRef]
18. Guo, L.; Feng, Y.; Li, X.; Wang, C.; Li, Y. Research on stability analysis and damping control methods for DC microgrid. *Proc. CSEE* **2016**, *36*, 927–936. [CrossRef]
19. Kesavan, V.S.; Gnanadass, N.D. Improved droop control strategy for parallel connected power electronic converter based distributed generation sources in an islanded microgrid. *Electr. Power Syst. Res.* **2021**, *201*, 107531. [CrossRef]
20. Li, Y.; Zhao, W.; Zhao, L.; Ma, K.; Lei, E.; Tan, L.; Jin, L.; Zhang, J.; Ma, Y.; Liu, S. Hybrid control strategy for peak shaving and frequency regulation based on battery energy storage SOC. *High Volt. Appar.* **2023**, *59*, 48–55+74. [CrossRef]
21. Wang, X.; Wang, H. Improved droop control strategy of multiple energy storage applications in an AC microgrid based on the state of charge. *Electronics* **2021**, *10*, 1726. [CrossRef]
22. Zhang, H.; Sun, S.; Feng, G.; Shi, B. Improved droop control strategy with fast equalization for SOC based on power balance in energy storage system. *IOP Conf. Ser. Mater. Sci. Eng.* **2019**, *563*, 032024. [CrossRef]
23. Zhang, X.; Hou, J.; Wang, Z.; Jiang, Y. Study of SOC estimation by the ampere-hour integral method with capacity correction based on LSTM. *Batteries* **2022**, *8*, 170. [CrossRef]
24. Li, P.; Zhang, C.; Yuan, R.; Kan, Z.; Chen, Y. Improve the load current distribution method of distributed energy storage systems with SOC droop control. *Proc. CSEE* **2017**, *37*, 3746–3754. [CrossRef]
25. Zhang, Y.; Luo, H.; Wang, Y. Research on Hybrid Energy Storage Power Allocation and Bus Voltage Stabilization in Photovoltaic DC Microgrid Based on Fuzzy-Drop Control. *Electr. Meas. Instrum.* **2023**, *60*, 51–58. [CrossRef]
26. Liu, X.; Lin, P.; Bu, F.; Zhuang, S.; Huang, S. Optimization of generator based on Gaussian process regression model with conditional likelihood lower bound search. *CES Trans. Electr. Mach. Syst.* **2024**, *8*, 32–42. [CrossRef]
27. Li, Y.; Dong, P.; Liu, M.; Yang, G.K. A distributed coordination control based on finite-time consensus algorithm for a cluster of DC microgrids. *IEEE Trans. Power Syst.* **2019**, *34*, 2205–2215. [CrossRef]
28. Xu, Y.L.; Li, X. Distributed optimal resource management based on the consensus algorithm in a microgrid. *IEEE Trans. Ind. Electron.* **2015**, *62*, 2584–2592. [CrossRef]
29. Ye, J.H.; Shi, D.; Qi, Y.S.; Gao, J.H.; Shen, J.X. Vibration suppression for active magnetic bearings using adaptive filter with iterative search algorithm. *CES Trans. Electr. Mach. Syst.* **2024**, *8*, 61–71. [CrossRef]

30. Huang, B.; Zheng, S.; Wang, R.; Wang, H.; Xiao, J.; Wang, P. Distributed optimal control of DC microgrid considering balance of charge state. *IEEE Trans. Energy Convers.* **2022**, *37*, 2174. [CrossRef]
31. Tian, X.; Chi, Y.; Li, L.; Liu, H. Review of the configuration and transient stability of large-scale renewable energy generation through hybrid DC transmission. *CES Trans. Electr. Mach. Syst.* **2024**, *8*, 115–126. [CrossRef]
32. Zhu, D.; Zhou, Q.; Jia, Y.; Meng, J.; Zhang, J. Dynamic optimization control strategy for distribution network voltage considering photovoltaic accommodation and energy storage SOC. *High Volt. Eng.* **2026**, 1–15. [CrossRef]
33. Guo, L.; Liu, X.; Li, X.; Wang, R.; Sun, Q. A distributed energy storage SOC accelerated balancing control strategy for DC microgrid to improve current sharing accuracy. *Control Decis.* **2025**, *40*, 2383–2390. [CrossRef]
34. Cheng, Z.; Ding, Q.; Chai, X. SOC balancing droop control based on improved droop coefficient. *Power Syst. Prot. Control* **2025**, *53*, 123–132. [CrossRef]
35. Liu, S.; Ye, J.; Li, J.; Yang, X.; Jiang, J. Review on defect problems in the production and service process of lithium-ion batteries. *Glob. Energy Interconnect.* **2025**, *8*, 326–335. [CrossRef]
36. Wang, Y.; Yang, H.; Li, J.; Huang, W.; Zhang, W.; Wang, L. Joint optimal dispatching of dual-source trolleybus and power grid considering battery aging. *Smart Power* **2026**, *54*, 47–57. [CrossRef]